Yu *et al. Energy Mater* 2022;2:200037
DOI: 10.20517/energymater.2022.42

Energy Materials

Article

Open Access

Enabling 4.6 V $LiNi_{0.6}Co_{0.2}Mn_{0.2}O_2$ cathodes with excellent structural stability: combining surface $LiLaO_2$ self-assembly and subsurface La-pillar engineering

Zhaozhe Yu[1,2], Qilin Tong[1], Yan Cheng[1,*], Ping Yang[1], Guiquan Zhao[1], Huacheng Li[1], Weifeng An[1], Dongliang Yan[1], Xia Lu[3,*], Bingbing Tian[2,*]

[1]Guangxi Key Laboratory of Manufacturing Systems and Advanced Manufacturing Technology, Guilin University of Electronic Technology, Guilin 541004, Guangxi Zhuang Autonomous Region, China.
[2]International Collaborative Laboratory of 2D Materials for Optoelectronics Science and Technology of Ministry of Education, Institute of Microscale Optoelectronics, Shenzhen University, Shenzhen 518060, Guangdong, China.
[3]School of Materials, Sun Yat-Sen University, Shenzhen 518107, Guangdong, China.

[*]**Correspondence to:** Dr. Yan Cheng, Guangxi Key Laboratory of Manufacturing Systems and Advanced Manufacturing Technology, Guilin University of Electronic Technology, No. 1 Jinji Road, Qixing District, Guilin 541004, Guangxi Zhuang Autonomous Region, China. E-mail: B12030015@hnu.edu.cn; Prof. Xia Lu, School of Materials, Sun Yat-Sen University, No. 66 Gongchang Road, Xinhu Street, Guangming District, Shenzhen 518107, Guangdong, China. E-mail: luxia3@mail.sysu.edu.cn; Prof. Bingbing Tian, International Collaborative Laboratory of 2D Materials for Optoelectronics Science and Technology of Ministry of Education, Institute of Microscale Optoelectronics, Shenzhen University, No. 3688 Nanhai Avenue, Nanshan District, Shenzhen 518060, Guangdong, China. E-mail: tianbb2011@szu.edu.cn

How to cite this article: Yu Z, Tong Q, Cheng Y, Yang P, Zhao G, Li H, An W, Yan D, Lu X, Tian B. Enabling 4.6 V $LiNi_{0.6}Co_{0.2}Mn_{0.2}O_2$ cathodes with excellent structural stability: combining surface $LiLaO_2$ self-assembly and subsurface La-pillar engineering. *Energy Mater* 2022;2:200037. https://dx.doi.org/10.20517/energymater.2022.42

Received: 29 Jul 2022 **First Decision:** 13 Sep 2022 **Revised:** 25 Sep 2022 **Accepted:** 10 Oct 2022 **Published:** 21 Oct 2022

Academic Editor: Yuping Wu **Copy Editor:** Fangling Lan **Production Editor:** Fangling Lan

Abstract

Although Ni-rich layered materials with the general formula $LiNi_{1-x-y}Co_xMn_yO_2$ ($0 < x, y < 1$, NCM) hold great promise as high-energy-density cathodes in commercial lithium-ion batteries, their practical application is greatly hampered by poor cyclability and safety. Herein, a $LiNi_{0.6}Co_{0.2}Mn_{0.2}O_2$ (NCM622) cathode modified with a surface self-assembling $LiLaO_2$ coating and subsurface La pillars demonstrates stabilized cycling at 4.6 V. The $LiLaO_2$-coated NCM622 benefits from the suppression of interfacial side reactions, which relieves the layer-to-rock salt phase transformation and therefore improves the capacity retention under high voltages. Moreover, the La dopant, as a pillar in the NCM622 lattice, plays a dual role in expanding the *c* lattice parameter to enhance the Li-ion diffusion capability, as well as suppressing Ni antisite defect formation upon cycling. Consequently, the dual-

modified NCM622 cathode exhibits an initial Coulombic efficiency of over 85% and a high capacity of over 200 mAh g^{-1} at 0.1 C. A specific capacity of 188 mAh g^{-1} with a capacity retention of 76% is achieved at 1 C after 200 cycles within a voltage range of 3.0-4.6 V. These findings lay a solid foundation for the materials design and performance optimization of high-energy-density cathodes for Li-ion batteries.

Keywords: $LiNi_{0.6}Co_{0.2}Mn_{0.2}O_2$ cathode, surface coating, La pillars, high energy density, Li-ion batteries

INTRODUCTION

Despite the rapid development of lithium-ion batteries (LIBs) in recent decades, their finite energy and power densities are regarded as the main barriers to their further application[1-4]. The cathode is the most critical component and is crucial in determining the working voltage, energy density and cost of a LIB[5-9]. Various promising cathode candidates with high capacity, including $LiCoO_2$ and Ni-rich materials, have been extensively designed for LIBs[10,11]. Among the available candidates, nickel-rich layered cathode materials, namely, $LiNi_xCo_yMn_{1-x-y}O_2$ (NCM, x ≥ 0.6), have demonstrated excellent market prospects owing to their advantages of high specific capacities, large discharge plateaus, low price and hypotoxicity[12-14]. Although the specific capacity of NCM materials increases significantly with the nickel content, the resulting cation mixing and interfacial side reactions lead to a rapid performance decay upon cycling. In addition, the NCM materials with more than a 70% nickel content manifest apparent safety concerns, thereby hindering their large-scale application[15-19]. The increasing cutoff voltage of NCM can also increase its specific capacity. For instance, the discharge capacity of $LiNi_{0.6}Co_{0.2}Mn_{0.2}O_2$ (NCM622) can be enhanced from 180 to 200 mAh g^{-1} with an increase in the cutoff voltage from 4.4 to 4.6 V. However, at 4.6 V, the surface side reactions and unamiable phase transitions increase in NCM significantly, resulting in capacity fading[20-24]. Furthermore, the surface lattice structure of NCM622 can suffer from the uncontrollable cation mixing, leading to an irreversible structural transformation and degradation.

Many approaches, including elemental doping and surface coating, have been adopted to overcome the aforementioned issues and enhance the structural stability of Ni-rich cathodes. Lattice doping using a variety of extrinsic ions, such as Ti[25], Na[26], Mg[27,28], Zr[29], Nb[30], Al[31] and La[32], has been already used to plausibly improve the electrochemical performance of NCM materials. Inorganic oxides, such as MgO[33], Al_2O_3[34], AlF_3[35], Li_3PO_4[36], SiO_2[37], In_2O_3[38], TiO_2[39], ZrO_2[40] and Li_2MnO_3[41], have been coated on the surface of NCM materials to alleviate the layer-to-rock salt phase transformation and improve the cycling stability. Furthermore, strategies of ion doping combined with surface modification have also been used to improve the electrochemical performance of NCM. Yang *et al.* used Ti doping and a La_4NiLiO_8 coating to significantly restrain the cation mixing of NCM811 and improve its capacity retention after 200 cycles[42]. Ming *et al.* employed Zr and Al doping of $LiNi_{0.83}Co_{0.12}Mn_{0.05}O_2$, which resulted in a remarkable enhancement in capacity and voltage retention[43]. However, the above studies focus mostly on the electrochemical performance of NCM materials in a lower potential range of 3.0-4.3 V. At an elevated voltage of 4.6 V, few reliable experimental results are available, and hence the underlying reaction mechanism concerning the capacity retention rate of NCM materials in this broader potential range is poorly understood[44-47].

La is a relatively inexpensive rare-earth material that is widely used in industry. The La-O bond has an energy of 798 kJ mol^{-1}, much higher than that for Ni-O (392 kJ mol^{-1}), Co-O (368 kJ mol^{-1}) and Mn-O (402 kJ mol^{-1}). Moreover, La-based oxides have excellent conductivity and thermal stability. As surface coating materials, it is reported that La-based oxides can improve the conductivity of NCM, inhibit the side reactions and alleviate the layer-to-rock salt transformation at high voltages[48-50]. On this basis, in this work,

we design a dual modification strategy to synthesize a NCM622 cathode with surface $LiLaO_2$ self-assembly in conjunction with subsurface La pillaring, as shown in Scheme 1. The $LiLaO_2$ coating on the surface of NCM622 is beneficial for inhibiting the side reactions between the cathode and electrolyte, thereby relieving the phase transformation from the layered to rock salt phase and improving the capacity retention at high voltages. The La dopant, as a pillar in the NCM622 lattice, increases the *c* lattice parameter to improve the Li-ion diffusion capability and suppress Ni antisite defect formation. Density functional theory (DFT) calculations confirm that the Li-ion diffusion and electronic conductivity are greatly enhanced in the dual-modified NCM622 compared with the pristine material. As a result, the dual-modified NCM622 exhibits excellent cycling stability at 4.6 V (over 200 mAh g^{-1} at 0.1 C, 188 mAh g^{-1} at 1 C and a 76% capacity retention during 200 cycles), which is much better than the pristine material (45% capacity retention after 200 cycles).

EXPERIMENTAL

Materials preparation. The $Ni_{0.6}Co_{0.2}Mn_{0.2}(OH)_2$ precursor was synthesized using a hydroxide coprecipitation method. The details of the coprecipitation process are displayed in the supporting information. NCM622 samples were prepared by mixing $Ni_{0.6}Co_{0.2}Mn_{0.2}(OH)_2$ precursors and Li_2CO_3 (Li:Ni ratio of 1:0.56). After calcined at 870 °C for 10 h, the samples were cooled to 570 °C and then sintered at 570 °C for 5 h in an oxygen atmosphere. NCM622-La samples were prepared by homogeneously mixing $Ni_{0.6}Co_{0.2}Mn_{0.2}(OH)_2$ precursors, Li_2CO_3 and La_2O_3 (Li:Ni:La ratio of 1:0.56:0.003) and then sintered according to the above process. The synthesized NCM622-La@LLO was a mixture of NCM622-La, Li_2CO_3 and La_2O_3 with the molar ratio of Ni: Li: La (0.6:0.003:0.003) in an agate mortar and then calcined at 870 °C for 10 h in an oxygen atmosphere.

Materials characterization. The structure and morphology of the samples were evaluated by X-ray diffraction (XRD, Rigaku DMAX 2500, Tokyo, Japan) with Cu Kα radiation and scanning electron microscopy (SEM, Hitachi S-4800, Tokyo, Japan), respectively. The lattice parameters of the samples were refined by Full Prof Suite software. High-resolution transmission electron microscopy (HR-TEM, Tecnai G2 F30) was conducted to further understand the microstructure of the samples. The chemical states of the main elements of the materials were analyzed by X-ray photoelectron spectroscopy (XPS, Thermo ESCALAB 250Xi spectrometer).

Electrochemical measurements. The cell in a coin configuration (CR2016) assembled with the cathode, separator, lithium plate and electrolyte in an argon-filled glove box was used to investigate the electrochemical properties. The cathode was fabricated by coating the slurry composed of the active material, carbon black and binder at a ratio of 80:10:10 wt.% on Al foil. The electrode mass loadings of NCM622, NCM622-La and NCM622-La@LLO were 1.20, 1.18 and 1.22 mg/cm^2, respectively. Li metal was used as the counter and reference electrodes. Celgard 2400 was used as the separator. The electrolyte was 1 M $LiPF_6$ in ethylene carbonate/dimethyl carbonate (1:1 by volume). The as-prepared cells were used for electrochemical measurements with Neware software. Cyclic voltammetry (CV) and AC impedance spectroscopy (0.01-105 Hz) were carried out using a multichannel potentiostat/galvanostat from Princeton Applied Research. The galvanostatic intermittent titration technique was conducted to evaluate the kinetic properties of the electrodes.

RESULTS AND DISCUSSION

The crystal structures of NCM622, La-doped NCM622 (NCM622-La) and La-doped and $LiLaO_2$-coated NCM622 (NCM622-La@LLO) were studied by XRD, as shown in Figure 1A-C. The diffraction peaks of the (003), (101), (104), (105), (107) and (113) planes are observed [Figure 1A] and indexed to the hexagonal

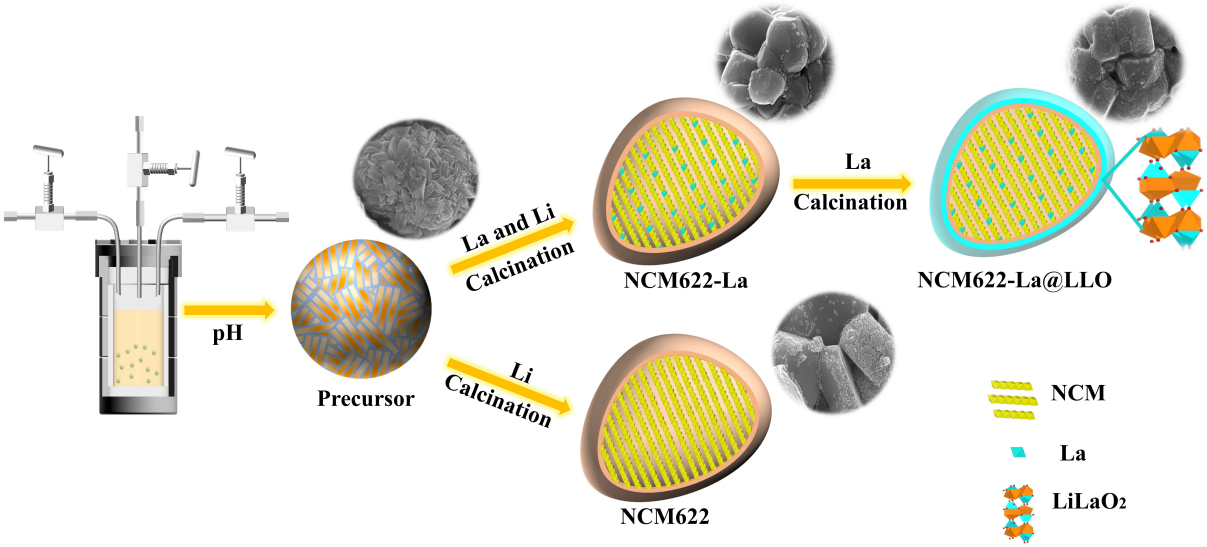

Scheme 1. Synthetic process of $LiNi_{0.6}Co_{0.2}Mn_{0.2}O_2$ (NCM622) cathode with and without modification.

$R\bar{3}m$ structure (PDF#09-0063), indicating that the doping and coating processes have no obvious influence on the crystal structure of NCM622. The separation of the (006)/(102) and (108)/(110) peaks illustrates a highly crystallized layered structure for the three samples[51]. The apparent left shift of the (104) peak of NCM622-La indicates that La successfully entered the NCM622 lattice [Figure 1C]. A similar phenomenon occurs on both the (104) and (003) peaks of NCM622-La@LLO [Figure 1B and C]. Additionally, the interplanar spacings of (003) and (104) widen, owing to the introduction of La, which is plausibly conducive to facilitating the ionic diffusion kinetics of Li ions[52,53]. Moreover, the weak diffraction peaks of (020), (111) and (220) observed in NCM622-La@LLO are attributed to the $LiLaO_2$ surface coating layer [Supplementary Figure 1].

XPS was used to evaluate the surface composition and oxidation states of the samples. As illustrated in Figure 1D-F, the peaks of Ni-$2p_{3/2}$ at 855.60 and 854.53 eV represent Ni^{3+} and Ni^{2+}, respectively. Apparently, compared to that in the pristine sample, the decrease in the Ni^{2+} content in both NCM622-La and NCM622-La@LLO is mainly due to the introduction of La^{3+}, whose electrostatic repulsion prevents more Ni^{2+} from migrating to the Li site, thereby inhibiting cation mixing[54,55]. The XPS analysis comparison of La in the three samples indicates that the La particles exist in both the NCM622-La and NCM622-La@LLO electrodes [Supplementary Figure 2]. The Rietveld refinement results further confirm that the Ni-Li cation mixing decreases after the La doping and $LiLaO_2$ coating [Supplementary Figure 3 and Supplementary Table 1].

The sizes of the NCM622-La@LLO particles are ~0.5 μm, smaller than that of the pristine NCM622 particles (~1 μm), as shown by the SEM images in Figure 1G-I. The introduction of La in the lithiation of the hydroxide precursor changes the surface energy, which changes the fusion of nanosheets during high-temperature calcination[56]. Interestingly, compared with the modified NCM622, many small particles appear on the surface of the original sample, which are residual lithium (Li_2CO_3/LiOH)[38]. The surface of the NCM622-La@LLO particles displays a blurred edge compared with the pristine NCM622 particles, preliminarily proving the $LiLaO_2$ formed on the surface of NCM622. Moreover, the integral morphologies of the three samples show no significant differences, indicating that the overall morphology of the host material is free from the destruction of the doping and coating processes [Supplementary Figure 4]. The energy-dispersive spectroscopy mapping images of NCM622 - La@LLO

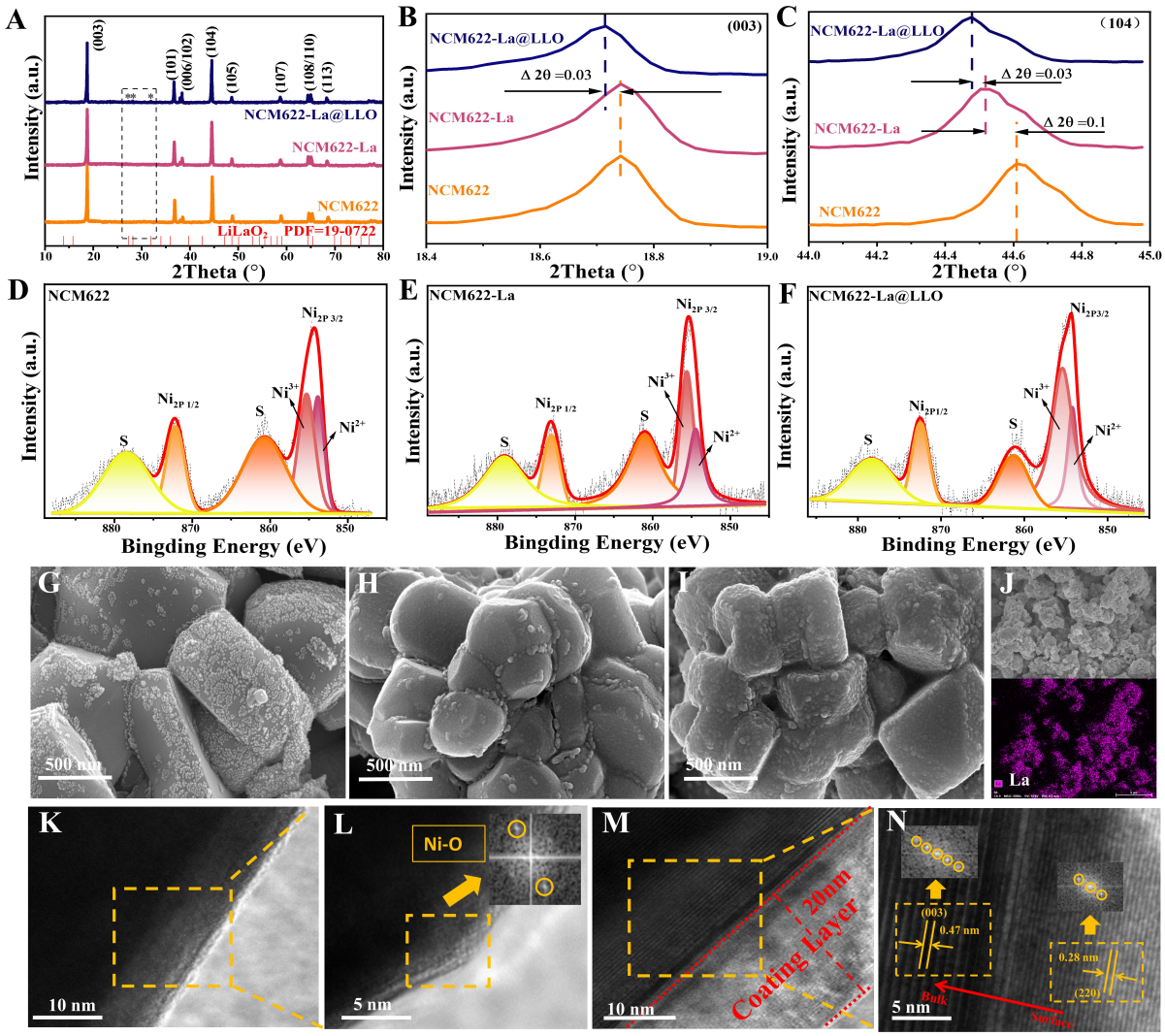

Figure 1. (A) XRD patterns of NCM622, NCM622-La and NCM622-La@LLO. (B and C) Comparison of (003) and (104) peaks for the three samples. (D-F) XPS comparison of Ni element for the three samples. (G-I) SEM morphology images of NCM622, NCM622-La and NCM622-La@LLO and (J) the corresponding energy-dispersive spectroscopy mapping results of NCM622-La@LLO. TEM images of (K and L) NCM622 and (M and N) NCM622-La@LLO.

[Figure 1J and Supplementary Figure 5] show a uniform distribution of La, indicating that $LiLaO_2$ is evenly coated on the surface of NCM622. Additionally, the HR-TEM images show that an obvious Ni-O phase exists on the pristine NCM622 electrode surface [Figure 1K and L] and the NCM622-La@LLO surface has a clear coating layer [Figure 1M]. The lattice fringes of the NCM622-La@LLO electrode vary significantly from the surface to the interior. The lattice spacing of the coating layer is 0.28 nm [Figure 1N], corresponding to the diffraction peak of the (220) plane of $LiLaO_2$, further confirming that the surface of NCM622-La@LLO is covered with a thin $LiLaO_2$ layer.

DFT calculations were used to estimate the surface structure of NCM622 before and after modification with La doping and $LiLaO_2$ coating, as shown in Figure 2A-I. Using the same structure, the calculated density of states (DOS) of NCM622-La@LLO is much larger than that of NCM622 and NCM622-La at the Fermi level [Figure 2D-F and Supplementary Figure 6], indicating that the electronic conductivity of NCM622-La@LLO

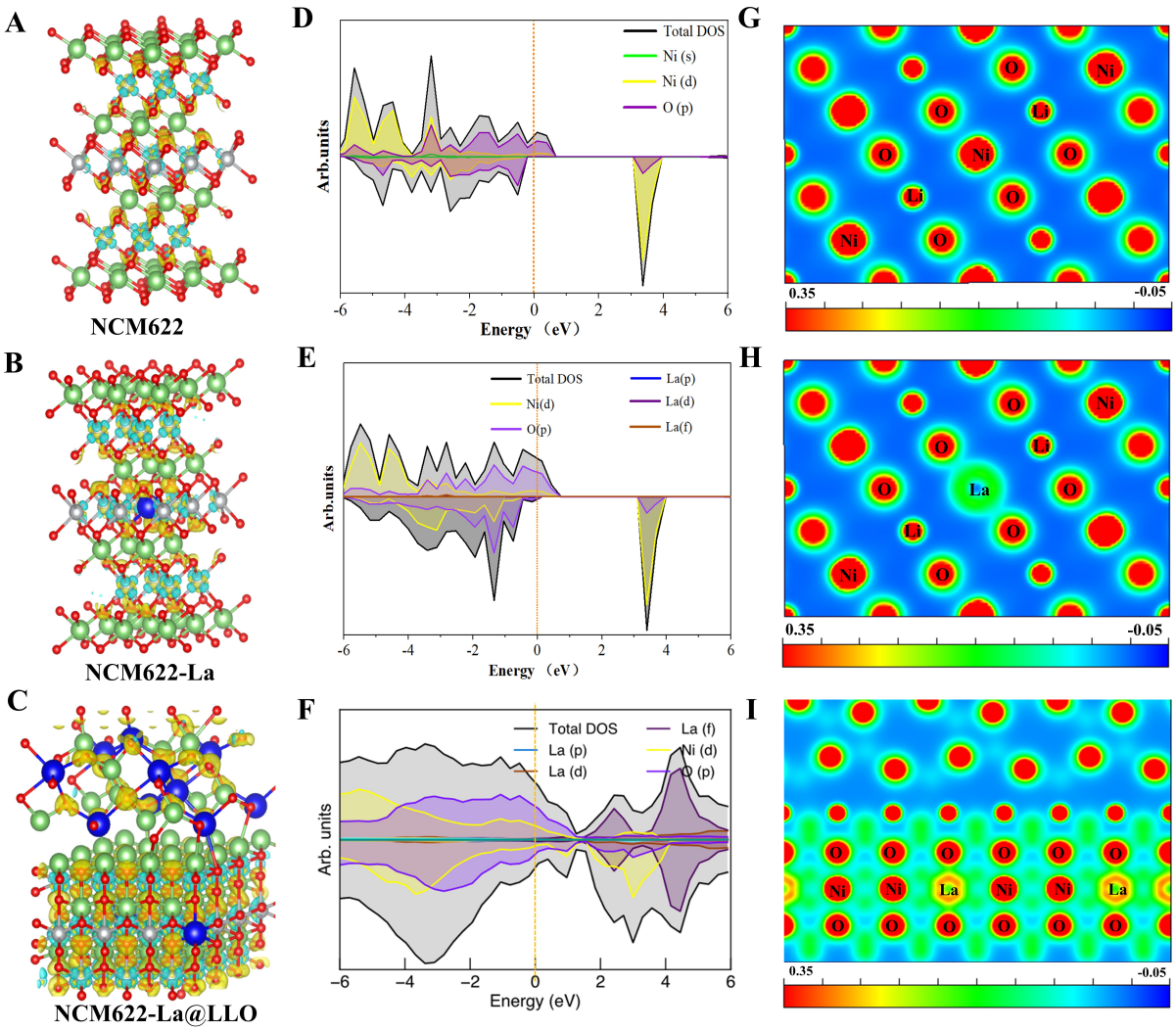

Figure 2. (A-C) Structural diagrams, (D-F) DOS and (G-I) differential charge densities of the three samples.

is improved[57]. Figure 2G-I and Supplementary Figures 7 and 8 exhibit the charge density differences between the three samples. An evident electron transfer phenomenon occurs among Ni, Co, La and the surrounding O atoms, and becomes clearer after La doping and $LiLaO_2$ coating. In addition, the La-O has a high electron aggregation degree compared to the Ni-O, suggesting that La-O has a stronger chemical bond, which will be beneficial to stabilize lattice oxygen during cycling, especially at a high cutoff voltage. Stable lattice oxygen can inhibit the layer-to-spinel/rock salt phase transformation and improve the electrochemical performance.

The ionic and electronic conductivities of NCM622, NCM622-La and NCM622-La@LLO measured with a blocking electrode method show that NCM622-La@LLO has the highest values [Figure 3A and B]. The Nyquist plots of the half-cells also reveal the best lithium-ion transport capability of NCM622-La@LLO [Figure 3C]. To understand the dynamic behavior of the three samples, the galvanostatic intermittent titration technique was used at a pulsed current of 20 mA/g [Supplementary Figure 9]. The lithium-ion diffusion coefficient in NCM622-La@LLO is estimated to be ~1.4×10^{-10} cm^2 s^{-1}, higher than that in NCM622 (5.1×10^{-12} cm^2 s^{-1}) and NCM622-La (4.0×10^{-11} cm^2 s^{-1}), suggesting that the La doping and $LiLaO_2$

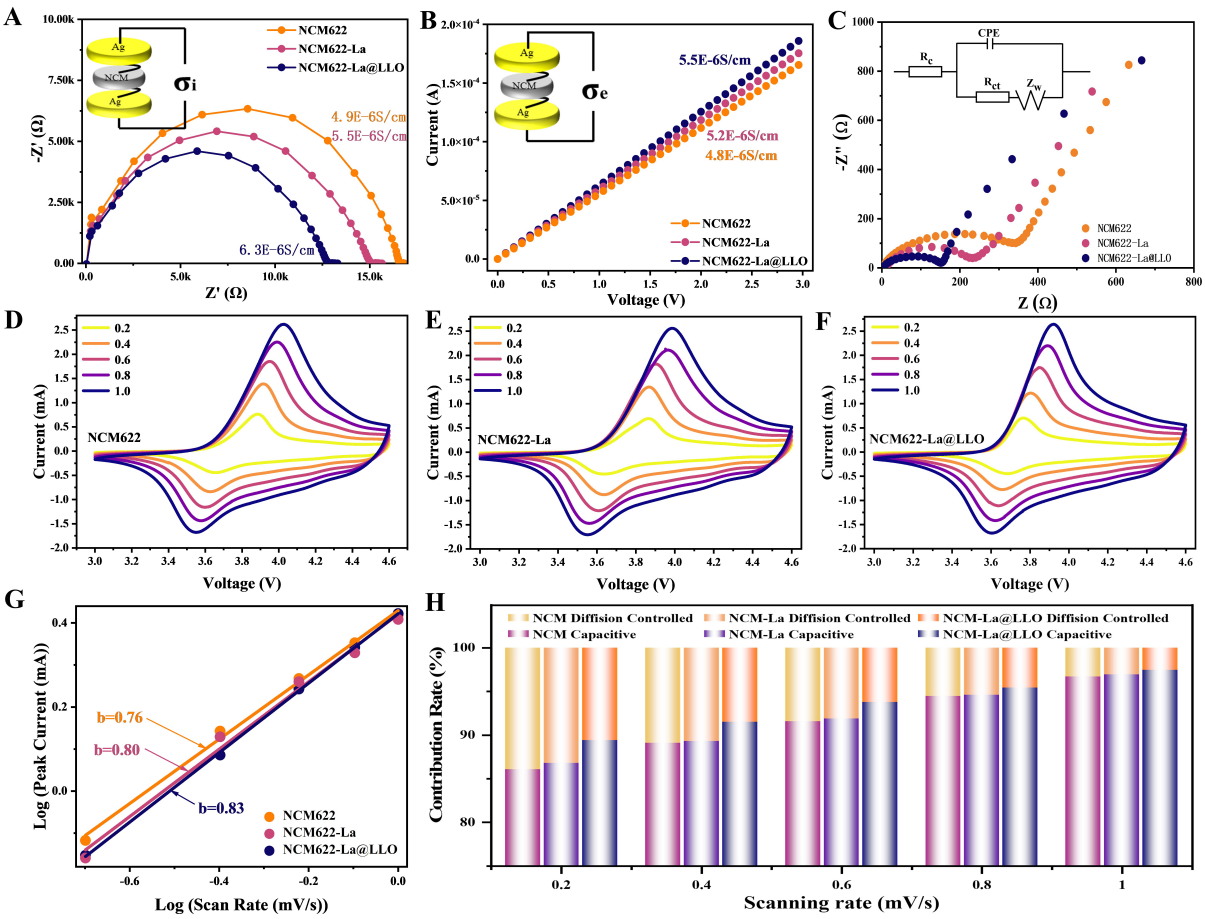

Figure 3. (A) Ionic and (B) electronic conductivity of NCM622, NCM622-La and NCM622-La@LLO samples. (C) Nyquist plots of the three electrodes. (D-F) CV curves of the three samples at different potential scanning rates. (G) Relationship between logarithmic anode peak current and logarithmic scan rates of the three electrodes. (H) Capacitance contribution calculations of the three electrodes at various scan rates.

coating boost the lithium-ion diffusion kinetics of NCM622. CV was carried out at a scan rate of 0.1 mV s^{-1} within the potential range of 3.0-4.6 V [Supplementary Figure 10]. The potential difference (ΔEp) values of the three samples between the oxidation/reduction peaks are 286 mV (NCM622), 187 mV (NCM622-La) and 166 mV (NCM622-La@LLO), respectively. The minimum positional deviation of the oxidation/deoxidization peaks indicates that NCM622-La@LLO exhibits the best electrochemical activity and cycle reversibility. The CV curves of the three samples at different potential scan rates from 0.2 to 1.0 mV s^{-1} are shown in Figure 3D-F. Both the oxidation and reduction peak currents of the three samples gradually increase with the scanning rate and shift toward low and high potentials, respectively. The fitting result indicates that the diffusion-controlled electrochemical process dominates the charge/discharge reaction in electrodes[58-60]. The *b* values of the cathode peaks of NCM622, NCM622-La and NCM622-La@LLO are 0.76, 0.80 and 0.83, respectively, indicating that the NCM622-La@LLO has more significant surface capacitive effects [Figure 3G]. Figure 3H distinguishes the percentage of the capacitive contribution and diffusion-controlled contribution for the three electrodes at different scan rates. Although the capacitive contribution increases with scan rate, the surface capacitive contribution of NCM622-La@LLO dominates, meaning that the capacitance control process plays an important role in Li-ion storage at higher scan rates[61].

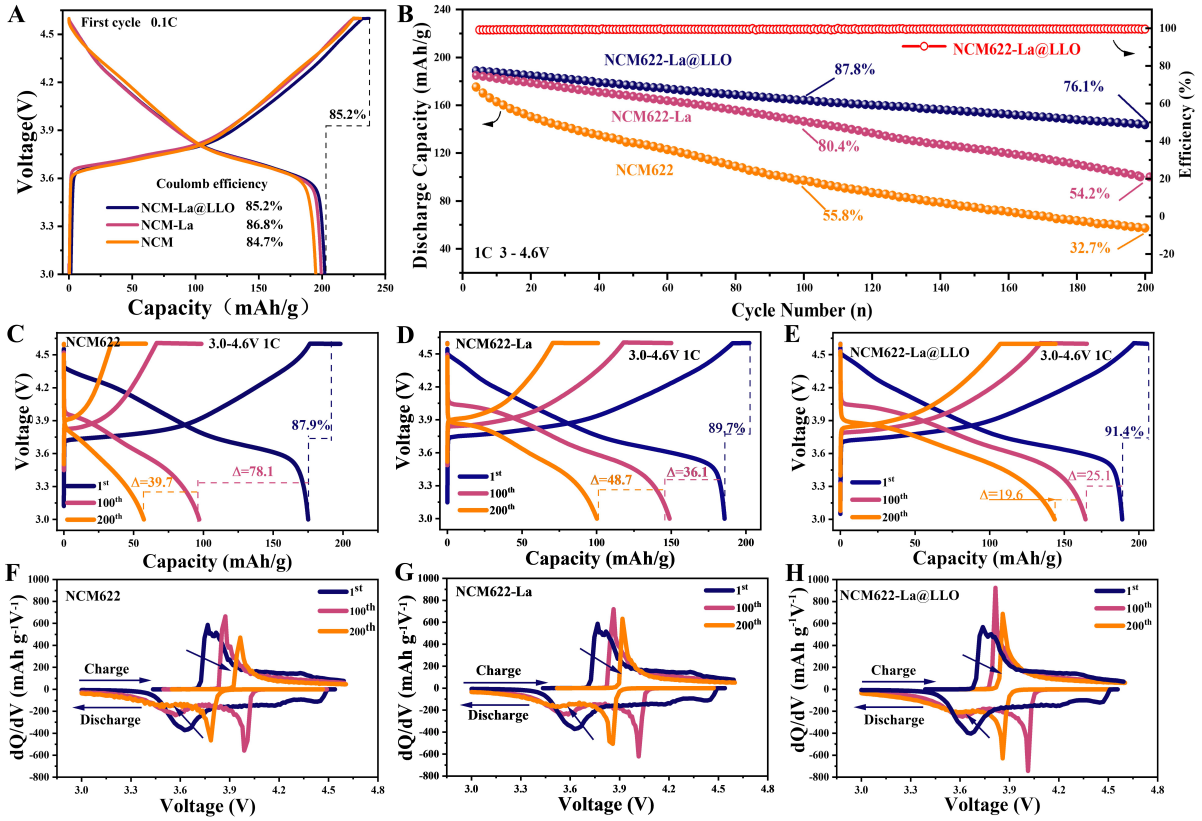

Figure 4. (A) Charge and discharge curves of the first cycles of NCM, NCM-La and NCM622-La@LLO at a current density of 20 mA g^{-1} (0.1 C) and (B) corresponding cycling performance at 1 C in the voltage range of 3.0-4.6 V. Charge and discharge curves of different cycles and corresponding dQ/dV curves of (C and F) NCM622, (D and G) NCM622-La and (E and H) NCM622-La@LLO.

The first-cycle discharge/charge capacities of NCM622-La@LLO are 237.2/202.2 mAh g^{-1}, with a corresponding initial Coulombic efficiency (ICE) of 85.2% [Figure 4A]. There is little difference among the ICEs compared with NCM622 (84.7%) and NCM622-La (86.8%) [Supplementary Figure 11], indicating that La doping and $LiLaO_2$ coating have little effect on the ICE of NCM622 materials. Figure 4B further compares the electrochemical cycling performances of the three samples after various cycles at 1 C. For NCM622-La@LLO, excellent capacity retention can be achieved at 76.1% after 200 cycles. In contrast, pristine NCM622 undergoes rapid capacity decay, resulting in a lower capacity retention of only 32.7% after 200 cycles. Furthermore, NCM622-La@LLO shows a good charge and discharge plateau above 3.6 V after 200 cycles [Figure 4C-E]. Figure 4F-H provides a detailed analysis of the evolution process of the differential capacitance (dQ/dV) curves of the three samples. The dQ/dV curves display two redox peaks during cycling. However, for the NCM622 sample, the intensity of the redox peak becomes weaker than that of the NCM622-La and NCM622-La@LLO samples when the cycle number increases, indicating that La-pillared and $LiLaO_2$-coated NCM622 exhibits a more stable structure, a stronger ability to withstand high voltages and better electrochemical performance.

The crystal structures and surface morphologies of the samples after 200 cycles were investigated by TEM and SEM, respectively. The TEM images of NCM-La@LLO show that although no rock-salt phase is observed on the NCM-La@LLO surface, it conserves a well-ordered layered structure [Figure 5B]. In contrast, the rock-salt phase exists on the surface region of NCM622 and the spinel phase is detected from the diffraction spots, as shown in Figure 5A. The NCM622 exhibits a salt-spinel-layered structure from the

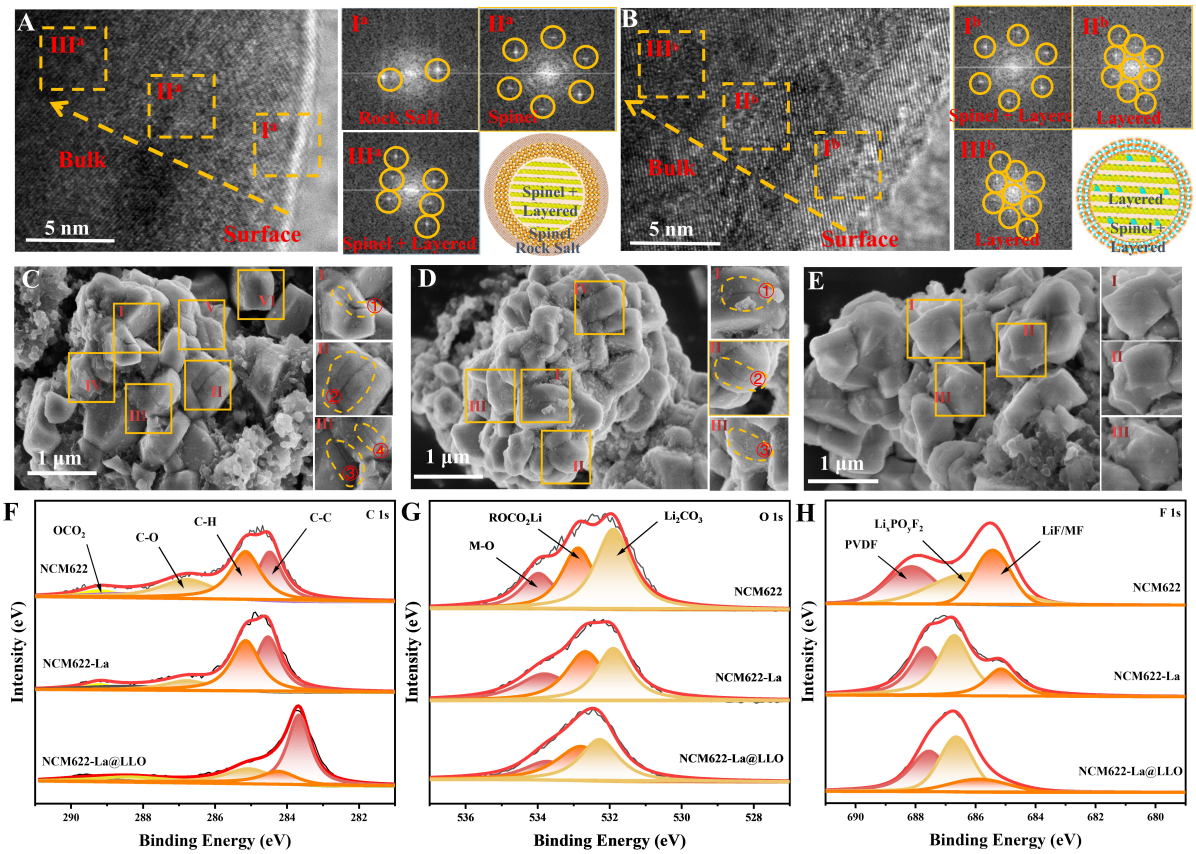

Figure 5. TEM images of (A) NCM622 and (B) NCM622-La@LLO after 200 cycles, where I^a, II^a, III^a, I^b, II^b and III^b are the fast Fourier transform conversion graphs of the corresponding regions. Surface morphologies of (C) NCM622, (D) NCM622-La and (E) NCM622-La@LLO after 200 cycles. (F) C1s, (G) O1s and (H) F1s XPS spectra of NCM622, NCM622-La and NCM622-La@LLO after 200 cycles.

surface to the inner phase, but the NCM-La@LLO exhibits a slight mixture of the layered and spinel phases on the surface. This obvious evidence indicates that La doping and $LiLaO_2$ coating significantly inhibit the transformation of the layered phase to the rock-salt phase and maintain the structural stability of the NCM material, thereby improving the reversible specific capacity and cycle life. The surface morphologies of NCM622-La@LLO after 200 cycles are shown in Figure 5E. Compared with the NCM622 and NCM622-La particles [Figure 5C and D], no cracks exist on the surface of NCM622-La@LLO, indicating that La doping and $LiLaO_2$ coating significantly inhibit the phase transition to maintain the structural stability of NCM at high voltages, thus improving the electrochemical performance.

To further verify the protective effect of the coating layers on the cathode-electrolyte interface, XPS measurements on NCM622, NCM622-La and NCM622-La@LLO after 200 cycles were conducted [Figure 5F-H]. The peaks of the C-H, C-C, C-O and OCO_2 bonds can be observed in the C 1s spectra of the electrodes [Figure 5F]. The binders and conductive substances in the electrode can cause the existence of C-H and C-C bonds, while the C-O and OCO_2 bonds are related to the decomposition of the electrolyte[62]. Compared to NCM622, weaker peak intensities are observed for the peaks associated with the C-O and OCO_2 of the NCM622-La@LLO cathode, suggesting a lower electrolyte decomposition amount on the surface. In addition, the typical peaks of M-O, Li_2CO_3 and $ROCO_2Li$ can also be observed in the O 1s spectra [Figure 5G]. The $ROCO_2Li$ peak of the NCM622-La@LLO electrode is smaller, meaning that the $LiLaO_2$ coating layer formed in NCM@LLO can inhibit the decomposition of the electrolyte and the formation of

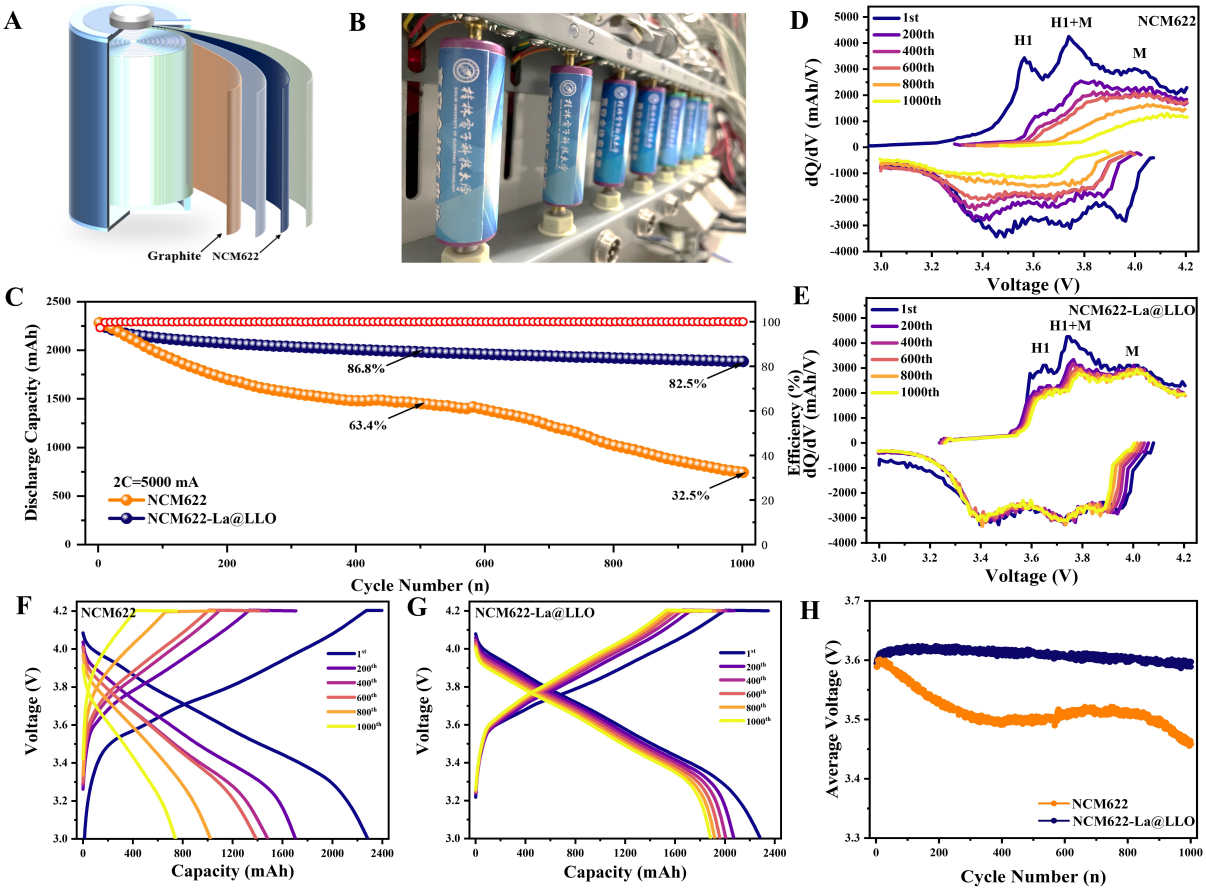

Figure 6. Electrochemical characterization of cylindrical full batteries. (A) Schematic and (B) photographs of the configuration of a graphite//NCM622-La@LLO full battery. (C) Cycling performance of full batteries with both pristine NCM622 and NCM622-La@LLO as the cathode and graphite as the anode at 2 C. (D and E) dQ dV^{-1} curves at selected cycles. (F and G) Corresponding charge/discharge curves. (H) Comparison of voltage platform attenuation.

SEI film on the particle surface during electrochemical cycling. Additionally, the LiF peak is significantly weakened in NCM622-La and almost invisible in NCM622-La@LLO, indicating that the La doping and $LiLaO_2$ coating significantly inhibit the surface side reactions and are helpful for the structural stability of NCM materials.

Cylindrical full batteries with a design capacity of 2500 mAh were assembled to compare the cycling stabilities of NCM622 and NCM622-La@LLO in real applications. Schematic diagrams of the cylindrical full batteries are shown in Figure 6A and B. The NCM622-La@LLO cell undergoes 1000 cycles with an excellent capacity retention of 82.5% [Figure 6C]. The overlap of the dQ/dV curves of the NCM622-La@LLO cathode demonstrates that La doping and $LiLaO_2$ coating can maintain the structural integrity of NCM materials [Figure 6D and E]. In addition, the charge/discharge curves from the 1st to 1000th cycle also suggest that the NCM622-La@LLO cathode has a higher reversible capacity due to the less electrochemical polarization compared with the NCM622 cathode [Figure 6F and G], which is mainly caused by the enhanced stability of NCM622 after La doping and $LiLaO_2$ coating. During long cycling [Figure 6H], the average voltage of the NCM622-La@LLO cell is stable at ~3.6 V, further proving the cyclic stability of the NCM622-La@LLO cathode. The excellent electrochemical performance of the NCM622-La@LLO cathode shows its excellent prospects for industrial applications.

CONCLUSIONS

In summary, we present a practical solution to enhance the stability of NCM622 at 4.6 V via the self-assembly of a $LiLaO_2$ coating on its surface and La pillars in its subsurface. The dual-modified NCM622-La@LLO cathode exhibits a capacity of more than 200 mAh g^{-1} and an initial Coulombic efficiency of 85% at a current density of 0.1 C. Even after 200 cycles, NCM622-La@LLO maintains a capacity retention of 1.7 times higher than the pristine material (76% *vs.* 45%) at 1 C and 4.6 V. Two factors are responsible for the superior electrochemical performance of the NCM622-La@LLO cathode. The first is that the $LiLaO_2$ coating on the surface of NCM622 is beneficial for inhibiting the side reactions between cathodes and electrolytes and suppressing the phase transformation from the layered phase to the rock-salt phase, thereby improving the capacity retention at high voltage. The other reason is that the La atom dopants, as pillars in the NCM622 lattice, increase the *c*-axis distance to improve the Li^+ diffusion rate, and suppress nickel taking the place of lithium. We expect this strategy could provide a direction for managing the internal structure and interfacial stability of NCM, which can be extended to the applications of other cathodes, such as $LiMn_{2x}Ni_xO_4$ spinel and layered Li-rich oxides.

DECLARATIONS

Authors' contributions

Methodology, formal analysis and writing manuscript: Yu Z, Cheng Y
Data analysis and technical support: Li H, An W
Data acquisition: Tong Q, Yang P, Zhao G
Supervision, writing - review and editing: Yan D, Lu X, Tian B

Availability of data and materials

The data supporting our findings can be found in the Supplementary Information.

Financial support and sponsorship

This study was financially supported by the Department of Science and Technology of Guangxi Province (Grant Nos.: AB21220027, AD19110090, AD19110077, and AA17204063), the Guangxi Natural Science Foundation (Grant Nos. 2020GXNSFAA159059, 2020GXNSFAA159037, and 2018GXNSFGA281001), Engineering Research Center Foundation of Electronic Information Materials and Devices (Grant No. EIMD-AA202005), and National Natural Science Foundation of China (Grant Nos. 21805055, 22075328, and 51974098).

Conflicts of interest

All authors declared that there are no conflicts of interest.

Ethical approval and consent to participate

Not applicable.

Consent for publication

Not applicable.

REFERENCES

1. Asadi M, Sayahpour B, Abbasi P, et al. A lithium-oxygen battery with a long cycle life in an air-like atmosphere. *Nature* 2018;555:502-6. DOI PubMed

2. Zhu X, Meng F, Zhang Q, et al. $LiMnO_2$ cathode stabilized by interfacial orbital ordering for sustainable lithium-ion batteries. *Nat Sustain* 2021;4:392-401. DOI
3. Niu Y, Yu Z, Zhou Y, et al. Constructing stable Li-solid electrolyte interphase to achieve dendrites-free solid-state battery: a nano-interlayer/Li pre-reduction strategy. *Nano Res* 2022;15:7180-9. DOI
4. Yu Z, Zhou L, Cheng Y, et al. Preset lithium source electrolyte boosts SiO anode performance for lithium-ion batteries. *ACS Sustain Chem Eng* 2022;10:10351-60. DOI
5. Pomerantseva E, Bonaccorso F, Feng X, Cui Y, Gogotsi Y. Energy storage: the future enabled by nanomaterials. *Science* 2019;366:eaan8285. DOI PubMed
6. Cheng Y, Wei K, Yu Z, et al. Ternary Si-SiO-Al composite films as high-performance anodes for lithium-ion batteries. *ACS Appl Mater Interfaces* 2021;13:34447-56. DOI PubMed
7. Chi X, Li M, Di J, et al. A highly stable and flexible zeolite electrolyte solid-state Li-air battery. *Nature* 2021;592:551-57. DOI PubMed
8. Ding Z, Zhang C, Xu S, et al. Stable heteroepitaxial interface of Li-rich layered oxide cathodes with enhanced lithium storage. *Energy Storage Mater* 2019;21:69-76. DOI
9. Yu Z, Tian B, Li Y, et al. Lithium titanate matrix-supported nanocrystalline silicon film as an anode for lithium-ion batteries. *ACS Appl Mater Interfaces* 2019;11:534-40. DOI PubMed
10. Feng X, Wu H, Gao B, Świętosławski M, He X, Zhang Q. Lithiophilic N-doped carbon bowls induced Li deposition in layered graphene film for advanced lithium metal batteries. *Nano Res* 2022;15:352-60. DOI
11. Ke C, Shao R, Zhang Y, et al. Synergistic engineering of heterointerface and architecture in new-type ZnS/Sn heterostructures in situ encapsulated in nitrogen-doped carbon toward high-efficient lithium-ion storage. *Adv Funct Mater* 2022;32:2205635. DOI
12. Fan X, Hu G, Zhang B, et al. Crack-free single-crystalline Ni-rich layered NCM cathode enable superior cycling performance of lithium-ion batteries. *Nano Energy* 2020;70:104450. DOI
13. Kim H, Kim MG, Jeong HY, Nam H, Cho J. A new coating method for alleviating surface degradation of $LiNi_{0.6}Co_{0.2}Mn_{0.2}O_2$ cathode material: nanoscale surface treatment of primary particles. *Nano Lett* 2015;15:2111-9. DOI PubMed
14. Hussain N, Li M, Tian B, Wang H. Co_3Se_4 quantum dots as an ultrastable host material for potassium-ion intercalation. *Adv Mater* 2021;33:e2102164. DOI
15. Tsai P, Wen B, Wolfman M, et al. Single-particle measurements of electrochemical kinetics in NMC and NCA cathodes for Li-ion batteries. *Energy Environ Sci* 2018;11:860-71. DOI
16. Kim JH, Ryu HH, Kim SJ, Yoon CS, Sun YK. Degradation mechanism of highly Ni-Rich Li[NixCoyMn$_{1-x-y}$]O_2 cathodes with x > 0.9. *ACS Appl Mater Interfaces* 2019;11:30936-42. DOI PubMed
17. Kim A, Strauss F, Bartsch T, et al. Stabilizing effect of a hybrid surface coating on a Ni-Rich NCM cathode material in all-solid-state batteries. *Chem Mater* 2019;31:9664-72. DOI
18. Heenan TMM, Wade A, Tan C, et al. Identifying the origins of microstructural defects such as cracking within Ni-Rich NMC811 cathode particles for lithium-ion batteries. *Adv Energy Mater* 2020;10:2002655. DOI
19. Yu Z, Qu X, Wan T, et al. Synthesis and mechanism of high structural stability of nickel-rich cathode materials by adjusting li-excess. *ACS Appl Mater Interfaces* 2020;12:40393-403. DOI PubMed
20. Fan X, Chen L, Ji X, et al. Highly fluorinated interphases enable high-voltage Li-metal batteries. *Chem* 2018;4:174-85. DOI
21. Zhu Z, Liang Y, Hu H, et al. Enhanced structural and electrochemical stability of $LiNi_{0.83}Co_{0.11}Mn_{0.06}O_2$ cathodes by zirconium and aluminum co-doping for lithium-ion battery. *J Power Sources* 2021;498:229857. DOI
22. Lee S, Kim M, Jeong JH, et al. Li_3PO_4 surface coating on Ni-rich $LiNi_{0.6}Co_{0.2}Mn_{0.2}O_2$ by a citric acid assisted sol-gel method: improved thermal stability and high-voltage performance. *J Power Sources* 2017;360:206-14. DOI
23. Han S, Zhang H, Fan C, Fan W, Yu L. 1,4-Dicyanobutane as a film-forming additive for high-voltage in lithium-ion batteries. *Solid State Ionics* 2019;337:63-9. DOI
24. Fu J, Mu D, Wu B, et al. Enhanced electrochemical performance of $LiNi_{0.6}Co_{0.2}Mn_{0.2}O_2$ cathode at high cutoff voltage by modifying electrode/electrolyte interface with lithium metasilicate. *Electrochim Acta* 2017;246:27-34. DOI
25. Yang J, Huang B, Yin J, et al. Structure integrity endowed by a ti-containing surface layer towards ultrastable $LiNi_{0.8}Co_{0.15}Al_{0.05}O_2$ for all-solid-state lithium batteries. *J Electrochem Soc* 2016;163:A1530-4. DOI
26. Wang Y, Sun Y, Liu S, Li G, Gao X. Na-Doped $LiNi_{0.8}Co_{0.15}Al_{0.05}O_2$ with excellent stability of both capacity and potential as cathode materials for li-ion batteries. *ACS Appl Energy Mater* 2018;1:3881-9. DOI PubMed
27. Yu Z, Tong Q, Zhao G, Zhu G, Tian B, Cheng Y. Combining surface holistic Ge coating and subsurface Mg doping to enhance the electrochemical performance of $LiNi_{0.8}Co_{0.1}Mn_{0.1}O_2$ cathodes. *ACS Appl Mater Interfaces* 2022;14:25490-500. DOI PubMed
28. Huang Y, Zhu Y, Fu H, et al. Mg-pillared $LiCoO_2$: towards stable cycling at 4.6 V. *Angew Chem Int Ed* 2021;60:4682-8. DOI PubMed
29. Xue W, Huang M, Li Y, et al. Ultra-high-voltage Ni-rich layered cathodes in practical Li metal batteries enabled by a sulfonamide-based electrolyte. *Nat Energy* 2021;6:495-505. DOI
30. Li J, Zhang M, Zhang D, Yan Y, Li Z. An effective doping strategy to improve the cyclic stability and rate capability of Ni-rich $LiNi_{0.8}Co_{0.1}Mn_{0.1}O_2$ cathode. *Chem Eng J* 2020;402:126195. DOI
31. Du F, Li X, Wu L, et al. Tailoring the Al distribution in secondary particles for optimizing the electrochemical performance of $LiNi_{0.8}Co_{0.1}Mn_{0.1}O_2$. *Ceramics Inter* 2021;47:12981-91. DOI

32. Zhang M, Wang C, Zhang J, Li G, Gu L. Preparation and electrochemical characterization of La and Al Co-doped NCM811 cathode materials. *ACS Omega* 2021;6:16465-71. DOI PubMed PMC
33. Yoon W, Nam K, Jang D, et al. Structural study of the coating effect on the thermal stability of charged MgO-coated $LiNi_{0.8}Co_{0.2}O_2$ cathodes investigated by in situ XRD. *J Power Sources* 2012;217:128-34. DOI
34. Hu D, Du F, Cao H, et al. An effective strategy to control thickness of Al_2O_3 coating layer on nickel-rich cathode materials. *J Electroanal Chem* 2021;880:114910. DOI
35. Woo S, Yoon CS, Amine K, Belharouak I, Sun Y. Significant improvement of electrochemical performance of AlF_3-Coated $LiNi_{0.8}Co_{0.1}Mn_{0.1}O_2$ Cathode Materials. *J Electrochem Soc* 2007;154:A1005. DOI
36. Song HG, Kim JY, Kim KT, Park YJ. Enhanced electrochemical properties of $Li(Ni_{0.4}Co_{0.3}Mn_{0.3})O_2$ cathode by surface modification using Li_3PO_4-based materials. *J Power Sources* 2011;196:6847-55. DOI
37. Cho W, Kim S, Song JH, et al. Improved electrochemical and thermal properties of nickel rich $LiNi_{0.6}Co_{0.2}Mn_{0.2}O_2$ cathode materials by SiO_2 coating. *J Power Sources* 2015;282:45-50. DOI
38. Liu Y, Tang L, Wei H, et al. Enhancement on structural stability of Ni-rich cathode materials by in-situ fabricating dual-modified layer for lithium-ion batteries. *Nano Energy* 2019;65:104043. DOI
39. Chen Y, Zhang Y, Chen B, Wang Z, Lu C. An approach to application for $LiNi_{0.6}Co_{0.2}Mn_{0.2}O_2$ cathode material at high cutoff voltage by TiO_2 coating. *J Power Sources* 2014;256:20-7. DOI
40. Ahn J, Jang EK, Yoon S, et al. Ultrathin ZrO_2 on $LiNi_{0.5}Mn_{0.3}Co_{0.2}O_2$ electrode surface via atomic layer deposition for high-voltage operation in lithium-ion batteries. *Appl Surf Sci* 2019;484:701-9. DOI
41. Huang X, Zhu W, Yao J, et al. Suppressing structural degradation of Ni-rich cathode materials towards improved cycling stability enabled by a Li_2MnO_3 coating. *J Mater Chem A* 2020;8:17429-41. DOI
42. Yang H, Wu H, Ge M, et al. Simultaneously dual modification of ni-rich layered oxide cathode for high-energy lithium-ion batteries. *Adv Funct Mater* 2019;29:1808825. DOI
43. Ming Y, Xiang W, Qiu L, et al. Dual elements coupling effect induced modification from the surface into the bulk lattice for ni-rich cathodes with suppressed capacity and voltage decay. *ACS Appl Mater Interfaces* 2020;12:8146-56. DOI PubMed
44. Wu L, Tang X, Rong Z, et al. Studies on electrochemical reversibility of lithium tungstate coated Ni-rich $LiNi_{0.8}Co_{0.1}Mn_{0.1}O_2$ cathode material under high cut-off voltage cycling. *Appl Surf Sci* 2019;484:21-32. DOI
45. Gan Z, Lu Y, Hu G, et al. Surface modification on enhancing the high-voltage performance of $LiNi_{0.8}Co_{0.1}Mn_{0.1}O_2$ cathode materials by electrochemically active $LiVPO_4F$ hybrid. *Electrochim Acta* 2019;324:134807. DOI
46. Fan Q, Lin K, Yang S, et al. Constructing effective TiO_2 nano-coating for high-voltage Ni-rich cathode materials for lithium ion batteries by precise kinetic control. *J Power Sources* 2020;477:228745. DOI
47. Li J, Wang J, Lu X, et al. Enhancing high-potential stability of Ni-rich $LiNi_{0.8}Co_{0.1}Mn_{0.1}O_2$ cathode with PrF3 coating. *Ceram Int* 2021;47:6341-51. DOI
48. Wang R, Zhang T, Zhang Q, Zheng M, Xu K, Yan W. Enhanced electrochemical performance of La and F co-modified Ni-rich cathode. *Ionics* 2020;26:1165-71. DOI
49. Yang J, Chen Y, Li Y, et al. A simple strategy to prepare the $La_2Li_{0.5}Al_{0.5}O_4$ modified high-performance ni-rich cathode material. *Mater Chem Phys* 2020;249:123135. DOI
50. Cheng Z, Lv F, Xu N, et al. Enhanced rate performance and cycle stability of $LiNi_{0.6}Co_{0.2}Mn_{0.2}O_2$ at high cut-off voltage by $Li_{6.1}La_3Al_{0.3}Zr_2O_{12}$ surface modification. *Appl Surf Sci* 2020;524:146556. DOI
51. Jung C, Kim D, Eum D, et al. New insight into microstructure engineering of Ni-rich layered oxide cathode for high performance lithium ion batteries. *Adv Funct Mater* 2021;31:2010095. DOI
52. Qu X, Huang H, Wan T, et al. An integrated surface coating strategy to enhance the electrochemical performance of nickel-rich layered cathodes. *Nano Energy* 2022;91:106665. DOI
53. Liu Y, Zeng T, Li G, et al. The surface double-coupling on single-crystal $LiNi_{0.8}Co_{0.1}Mn_{0.1}O_2$ for inhibiting the formation of intragranular cracks and oxygen vacancies. *Energy Storage Mater* 2022;52:534-46. DOI
54. Han B, Xu S, Zhao S, et al. Enhancing the structural stability of Ni-Rich layered oxide cathodes with a preformed Zr-concentrated defective nanolayer. *ACS Appl Mater Interfaces* 2018;10:39599-607. DOI PubMed
55. Liu S, Chen X, Zhao J, et al. Uncovering the role of Nb modification in improving the structure stability and electrochemical performance of $LiNi_{0.6}Co_{0.2}Mn_{0.2}O_2$ cathode charged at higher voltage of 4.5 V. *J Power Sources* 2018;374:149-57. DOI
56. Kim U, Park G, Son B, et al. Heuristic solution for achieving long-term cycle stability for Ni-rich layered cathodes at full depth of discharge. *Nat Energy* 2020;5:860-9. DOI
57. Fan X, Ou X, Zhao W, et al. In situ inorganic conductive network formation in high-voltage single-crystal Ni-rich cathodes. *Nat Commun* 2021;12:5320. DOI PubMed PMC
58. Wei K, Zhou L, Wang S, et al. Watermelon-like texture lithium titanate and silicon composite films as anodes for lithium-ion battery with high capacity and long cycle life. *J Alloys Compd* 2021;885:160994. DOI
59. Shi Y, Zhang Z, Jiang P, et al. Unlocking the potential of P3 structure for practical Sodium-ion batteries by fabricating zero strain framework for Na+ intercalation. *Energy Storage Mater* 2021;37:354-62. DOI
60. Yu Z, Yu K, Wei J, Lu Q, Cheng Y, Pan Z. Improving electrode properties by sputtering Ge on SiO anode surface. *Ceram Int* 2022;48:26784-90. DOI
61. Yu Z, Zhou L, Tong J, Guan T, Cheng Y. Improving electrochemical performance of thick silicon film anodes with implanted solid

lithium source electrolyte. *J Phys Chem Lett* 2022;13:8725-32. DOI PubMed

62. Yang G, Pan K, Lai F, et al. Integrated co-modification of PO43- polyanion doping and Li_2TiO_3 coating for Ni-rich layered $LiNi_{0.6}Co_{0.2}Mn_{0.2}O_2$ cathode material of Lithium-Ion batteries. *Chem Eng J* 2021;421:129964. DOI